Geophys. J. Int. (1993) **112,** 264–275

Multiple forward scattering of surface waves: comparison with an exact solution and Born single-scattering methods

Wolfgang Friederich, Erhard Wielandt and Stefan Stange
Institut für Geophysik der Universität Stuttgart, Richard Wagner Str. 44, 7000 Stuttgart, Germany

Accepted 1992 July 31. Received 1992 July 15; in original form 1992 February 7

SUMMARY

We present a 2-D reformulation of surface wave scattering theory in terms of potentials, which allows an extension of the Born single-scattering approach to include multiple forward scattering. No additional numerical effort compared to single scattering is required for a computation of the wavefield over the whole heterogeneous region. Born single scattering for elastic surface waves and both multiple and single scattering for acoustic waves are also covered by the formulation. It is valid for fully anisotropic perturbations of the reference medium. We use the flexibility of our formulation to compare the different approximations with each other and, additionally, test all of them against an exact solution for the particular case of a cylindrical inclusion in a layered waveguide.

Our numerical results, obtained for shear velocity contrasts of about 6 per cent, show that the method which includes multiple scattering is superior to the single-scattering methods if the scattering region extends over more than one wavelength. If coupling to higher modes is suppressed, the multiple-scattering method still yields nearly exact results for the vertical displacement. The influence of mode coupling and type conversion leads to only small errors in vertical displacement. Moreover, as we show for a cylinder with a diameter of two wavelengths, even an acoustic treatment of surface waves including multiple forward scattering may be more accurate than single scattering within an elastic treatment. For scatterer sizes below one wavelength the single-scattering approaches are accurate enough, while elastic and acoustic treatments of surface waves may differ considerably.

The proposed multiple-scattering method is numerically very efficient, because the numerical effort mainly depends on the degrees of smoothness of the wavefield and the heterogeneity, and is not directly coupled to the wavelength.

Key words: multiple forward scattering, single scattering, surface waves.

1 INTRODUCTION

Important progress in surface wave scattering theory in the last few years was made by Kennett (1984) and Odom (1986) who introduced the coupled-mode theory, and by Snieder (1986a) who developed an elegant formulation of Born scattering theory for elastic surface waves. The coupled-mode method has been applied by Kennett & Mykkeltveit (1984) to study the propagation of *Lg*-waves across the Central Graben in the North Sea. Bostock (1991, 1992) has recently extended the coupled-mode method to 3-D structures, but with the limitation that the heterogeneity be composed of cylindrical shells in the radial direction. The Born scattering theory of Snieder is quite flexible as it allows the treatment of surface wave propagation across general 3-D structures with reasonable numerical effort by constraining the number of modes involved in coupling and conversion. Furthermore, Born scattering is ideally suited to inversion, since the scattered wavefield depends linearly on the structural perturbations. On the other hand, it is well known that Born single scattering may be a poor approximation if the region where scattering occurs is too large.

For practical reasons, the use of a purely numerical 3-D solution to interpret surface wave data is far from feasible. Hence one currently has to choose between two

approximate methods; 2-D mode-coupling theory, which stresses a correct modelling of coupling and conversion and results in a detailed picture of the vertical variations of the wavefield, but does not include lateral effects such as diffraction; and scattering theory, which focuses on the horizontal variations of the wavefield. Which aspect of the wavefield is more important for a structural interpretation? The answer certainly depends on the tectonic situation in which the recordings are made. For example, at continental margins, large faults or graben structures, mode coupling or conversion certainly plays an important role (Gregersen 1978; Kennett & Mykkeltveit 1984; Stange & Friederich 1992a) and a 2-D treatment appears appropriate. For structures acting more as scatterers than as reflectors or refractors, lateral propagation phenomena gain importance. As shown by Stange & Friederich (1992b), for the vertical displacement, scattering of the incoming mode on to itself dominates the wavefield and mode coupling is of only minor importance. Thus in smoothly heterogeneous 3-D structures Born scattering should be favoured.

We know that Born scattering is nearly exact if the scatterer is small compared to the wavelength. However, consider for example Central Europe where, with the German Regional Network (GRN) and the NARS array, we have the opportunity to obtain detailed information about earth structure. Presuming the existence of lateral heterogeneities in the whole area in which stations are installed, the heterogeneous region would have a diameter of about 1000 km, which is about six wavelengths at a period of 50 s. In such circumstances, is Born single scattering still accurate enough?

In this paper we present a method which gives reliable estimates of the surface wavefield for both small *and* smooth extended scatterers. It is an enhanced Born scattering method, which includes multiple scattering in the forward direction. We compare our method with different Born single-scattering methods, and test each method against an exact solution from Stange & Friederich (1992b).

2 SURFACE WAVE SCATTERING THEORY USING POTENTIALS: GENERAL PERTURBATIONS

Our starting point is the elastic wave equation in the frequency domain:

$$[-\partial_k(c_{ikjl}\,\partial_l) - \rho\omega^2\,\delta_{ij}]u_j = 0. \tag{1}$$

Here c_{ikjl} are the components of the elasticity tensor, ρ is density, ω is angular frequency and u_j are the components of the displacement vector. ∂_l denotes differentiation with respect to the coordinate x_l. We also use the notation (x, y, z) for the coordinates which correspond to (x_1, x_2, x_3). Where convenient, we change from component notation to vector notation using bold-face letters. In the above and all the following equations, the summation convention is used for lower indices, while for upper indices sums are written out explicitly. We use lower indices to denote components of vectors or tensors and upper indices to distinguish between different modes. Numbers as superscripts are always understood as exponents. For example, ω^2 means ω squared.

We are looking for solutions of equation (1) for a layered, laterally heterogeneous half-space. We use a right-handed coordinate system with x- and y-axes in the horizontal plane and the z-axis pointing into the half-space. As a first step, we split displacement and material parameters into a reference and a perturbed part:

$$c_{ikjl} = c^{(0)}_{ikjl} + \gamma_{ikjl}, \qquad u_j = u^{(0)}_j + v_j, \qquad \rho = \rho^{(0)} + \Delta\rho. \tag{2}$$

Here, $u^{(0)}_j$ may for instance be regarded as the incoming wave, while v_j represents the scattered wave. If equation (2) is inserted into the equation of motion (1), one obtains

$$[-\partial_k(c^{(0)}_{ikjl}\,\partial_l) - \rho^{(0)}\omega^2\,\delta_{ij}]v_j = [\partial_k(\gamma_{ikjl}\,\partial_l) + \omega^2\Delta\rho\,\delta_{ij}]u_j. \tag{3}$$

Here, it is assumed that $u^{(0)}_j$ is a solution of the elastic wave equation for the reference medium. With the Green function of the reference differential operator, equation (3) may be transformed to the equivalent integral equation

$$v_r(\mathbf{x}) = \int_V G_{ri}(\mathbf{x}, \mathbf{x}')[\partial'_k(\gamma_{ikjl}\,\partial'_l) + \omega^2\Delta\rho\,\delta_{ij}]u_j(\mathbf{x}')\,d^3\mathbf{x}'. \tag{4}$$

The prime on ∂ denotes differentiation with respect to primed coordinates. $\mathbf{x}'$ and $\mathbf{x}$ are the radius vectors of scattering point and observation point, respectively. The integration volume encloses all regions where lateral heterogeneities are present. In principle, the Green function contains all types of waves which may exist in the reference medium. But, since we are interested in surface wave scattering, we only use the surface wave part of the Green function. In an isotropic or transversely isotropic medium, this reduced Green function may be written (Takeuchi & Saito 1972)

$$G_{ri}(\mathbf{x}, \mathbf{x}') = \sum_n \left[U^n(z)\delta_{r3} - \frac{1}{k^n} V^n(z)\partial_r - \frac{1}{k^n} W^n(z)\epsilon_{r3k}\,\partial_k \right] g^n_i(x, y, \mathbf{x}'), \tag{5}$$

with g^n_i given by

$$g^n_i(x, y, \mathbf{x}') = \frac{-i}{8c^n c^n_g J^n_1}\left[U^n(z')\delta_{i3} - \frac{1}{k^n} V^n(z')\partial'_i - \frac{1}{k^n} W^n(z')\epsilon_{i3k}\,\partial'_k \right] H^{(2)}_0(k^n R). \tag{6}$$

Here, ϵ_{ijk} is the completely antisymmetric tensor of third order whose components are $+1$ if (i, j, k) is an even permutation of $(1, 2, 3)$, -1 if (i, j, k) is an odd permutation of $(1, 2, 3)$ and zero otherwise. U^n and V^n are the vertical eigenfunctions of the nth Rayleigh mode, while W^n denotes a Love-mode eigenfunction. To preserve generality, we do not distinguish between Love and Rayleigh modes, but instead consider them as elements of one set. If, for instance, mode n is a Love mode, U^n and V^n are assumed to be zero. If mode n is a Rayleigh mode, W^n is taken to be zero. k^n is the wavenumber and c^n and c^n_g are phase and group velocity of the corresponding mode. J^n_1 is a normalization integral given by

$$J^n_1 = \tfrac{1}{2}\int_0^\infty dz\rho^{(0)}[(U^n)^2 + (V^n)^2 + (W^n)^2]. \tag{7}$$

Finally, $H^{(2)}_0$ is the Hankel function of the second kind and zeroth order, and R is the distance between the scattering point $\mathbf{x}'$ and the observation point $\mathbf{x}$.

In the same way as the Green function we may write the displacements **u** and **v** as sums of modes:

$$v_r(\mathbf{x}) = \sum_n \left[U^n(z)\delta_{r3} - \frac{1}{k^n} V^n(z)\partial_r - \frac{1}{k^n} W^n(z)\epsilon_{r3k}\,\partial_k \right] \Phi_S^n(x, y) \tag{8}$$

and

$$u_r(\mathbf{x}') = \sum_m u_r^m = \sum_m \left[U^m(z')\delta_{r3} - \frac{1}{k^m} V^m(z')\partial'_r - \frac{1}{k^m} W^m(z')\epsilon_{r3k}\,\partial'_k \right] \Phi^m(x', y'). \tag{9}$$

Here, Φ_S^n is the scattered potential of mode n, while Φ^m is the potential of the total displacement of mode m. By inserting equations (8) and (5) into (4), we obtain an expression for the scattered potential of mode n generated by mode m:

$$\Phi_S^{nm}(x, y) = \int_V g_i^n(x, y, \mathbf{x}')[\partial'_k(\gamma_{ikjl}\,\partial'_l) + \omega^2\Delta\rho\delta_{ij}] \times u_j^m(\mathbf{x'})\, d^3\mathbf{x}'. \tag{10}$$

Finally, assuming that the heterogeneities are buried, application of Gauss theorem leads to the set of integral equations

$$\Phi_S^{nm}(x, y) = \int_V [(-\partial'_k g_i^n)(\gamma_{ikjl}\,\partial'_l u_j^m) + \omega^2\Delta\rho g_i^n u_i^m]\, d^3\mathbf{x}'. \tag{11}$$

The scattered potential Φ_S^n of mode n may be retrieved from Φ_S^{nm} by summing over m. The integral equations (11) are still exact, at least as exact as the Greens functions are. An approximate numerical solution can be obtained after two simplifying steps: the *a priori* unknown modal displacement field u_i^m must be replaced by a known estimate, and the integral discretized into a sum. With a suitable formulation of these two steps, we can make the method applicable both to isolated small scatterers and to extended smooth anomalies of the structure.

3 INTEGRAL EQUATIONS FOR THE SCATTERING POTENTIALS

In the classical Born approximation, u_i^m in equation (11) is replaced by the incident, undisturbed field. This approximation fails when the anomalous region is so large and uniform that the true displacement gets out of phase with the incident field. In this case, multiple forward scattering within the anomalous region must be taken into account. This could be done by iterating the solution of equation (11), but this is computationally awkward; we propose a somewhat less precise but much simpler approach.

In modelling surface waves from teleseismic sources, we can in general assume that the wavefield propagates roughly as a plane wave through the region of interest. We adjust the x-axis of our coordinate system in the general direction of propagation (the structure must be parametrized accordingly). Then, if the anomalies are smooth and if the wavefield is indeed roughly plane, derivatives of u_i^m with respect to y are negligible compared with derivatives with respect to x, and we obtain from equation (9) that

$$u_j^m = [U^m(z')\delta_{j3} + i\delta_{j1}V^m(z') + i\delta_{j2}W^m(z')]\Phi^m(x', y') = S_j^m(z')\Phi^m(x', y'). \tag{12}$$

S_j^m is introduced as an abbreviation defined by the corresponding expressions in the line above. Furthermore, we obtain approximately (see equation 11)

$$\gamma_{ikjl}\,\partial'_l u_j^m = (\gamma_{ikj3}\,\partial'_3 S_j^m - ik^m\gamma_{ikj1}S_j^m)\Phi^m,$$

allowing us to write for the scattered potential

$$\Phi_S^{nm} = \int_V d^3\mathbf{x}'[(\partial'_k g_i^n)(-\gamma_{ikj3}\,\partial'_3 S_j^m + ik^m\gamma_{ikj1}S_j^m) + \omega^2\Delta\rho g_i^n S_i^m]\Phi^m(x', y'). \tag{13}$$

In this form the scattering problem is essentially 2-D, because the z-dependence of the expression in square brackets is known *a priori*. Thus we may carry out the z-integration in advance and collect these terms in the scattering kernel

$$K_P^{nm}(x, y, \mid x', y') = \int dz'[(\partial'_k g_i^n)(-\gamma_{ikj3}\,\partial'_3 S_j^m + ik^m\gamma_{ikj1}S_j^m) + \omega^2\Delta\rho g_i^n S_i^m]. \tag{14}$$

The subscript P indicates that K_P is the kernel for a point scatterer. The system of integral equations may now simply be written

$$\Phi_S^{nm}(x, y) = \iint dx'\, dy' K_P^{nm}(x, y \mid x', y')\Phi^m(x', y'). \tag{15}$$

We have thus transformed the numerically awkward integral equation (11) to a 2-D standard integral equation with a kernel which contains all details of the scattering problem considered. For a different structure or a different approximation, we have only to exchange the scattering kernel!

Equation (15) may be interpreted as follows. Each point (x', y') acts as a point scatterer which, excited by the field Φ^m, radiates a scattered field $K_P^{nm}\Phi^m$. Integration over the anomalous region then yields the total scattered field. Now, if discretizing the integral naively, one would divide the medium into cells within which both the wavefield Φ^m and the kernel K_P could be considered as constant. However, this procedure would require very small cells, since both the scattering kernel and the wavefield oscillate rapidly according to the wavenumber k^m.

We follow here a more physical approach. Instead of requiring a constant wavefield within each cell, we only require a constant amplitude and, additionally, we specify how the phase changes within the cell. In our case, the obvious choice is to assume the wavefield in each cell to be a plane wave propagating in the x-direction:

$$\Phi^m(x', y') = \Phi^m(p', q')\exp[-ik^m(x' - p')], \tag{16}$$

where (p', q') denotes the coordinates of the centre of the cell. We call this assumption the *piecewise-plane-wave* approximation, because in each cell the true phase front is approximated by a straight line perpendicular to the dominant direction of propagation. We can now compute a

scattering kernel for each cell:

$$K_C^{nm}(p, q \mid p', q') = \int_{\text{cell}} dx'\, dy' K_P^{nm}(p, q \mid x', y') \times \exp[-ik^m(x' - p')]. \quad (17)$$

By multiplying this kernel by $\Phi^m(p', q')$ and summing over all cells, we get the scattered field due to mode m:

$$\Phi_S^{nm} = \sum_{p',q'} K_C^{nm}(p, q \mid p', q')\Phi^m(p', q'). \quad (18)$$

The great advantage of this formulation is that K_C does not depend on the current value of the wavefield and may therefore be computed in advance.

For a numerical evaluation of the scattering kernel K_C, the definition of equation (17) is unfavourable because of sidelobes caused by the edges of the cell. We circumvent this difficulty by integrating over a square with an area double that of the cell, in which the elastic parameters are smoothed by a squared cosine taper in both the x- and y-directions. Due to the squared cosine, the tapers of two neighbouring cells just overlap in such a way as to produce a constant value between their maxima. Thus by assembling several cells one can exactly represent a constant anomaly.

How large is the error introduced by neglecting the fact that the wavefield within a cell might be either non-plane or not propagating in the x-direction? Non-planeness can be excluded by simply choosing the cells to be small enough. Moreover, if the true propagation direction slightly deviates from the x-direction, we only commit a second-order error in the scattered field, because the amplitude and phase of the scattered wave both have an extremum in the forward direction. Sideways-scattered waves will interfere destructively if the medium is smooth enough. Note that the size of the cells is constrained by the request for planeness of the phasefront and constancy of the amplitude within each cell. Both requests are not necessarily coupled to the wavelength.

4 INCLUSION OF MULTIPLE FORWARD SCATTERING

The accuracy of our approach now crucially depends, aside from the validity of the approximations introduced above, on our estimate of the total wavefield Φ^m. For instance, if we substitute for Φ^m the reference potential of mode m, we obtain the classical Born approximation of Snieder (1986a), here formulated in terms of potentials. If, however, the wavefield is to be computed over the whole heterogeneous region, one may as well include multiple forward scattering without any additional effort.

Let us assume an incoming plane wave (see Fig. 1). Using the pre-computed scattering kernels, we first compute the scattered field originating from the row of cells nearest to the source, substituting the incident field for Φ^m. The scattered field is added, separately for each mode, to the incident field at all other rows. Then we compute and add the field scattered from the second row. But now we use the updated value of the modal field in this row when computing the scattered field. This procedure is repeated for all subsequent rows. Since we always use the most recent value of the modal field to compute the scattered field, all multiply scattered waves from previous rows are included. Backward-scattered waves contribute to the final result but are not scattered again; their phase may therefore be incorrect at greater distances from the scattering cell. This simplified treatment of backward-scattered waves should nevertheless be adequate for two extreme types of anomaly: isolated small scatterers for which multiple scattering can be neglected, and extended smooth anomalies for which backward scattering is insignificant.

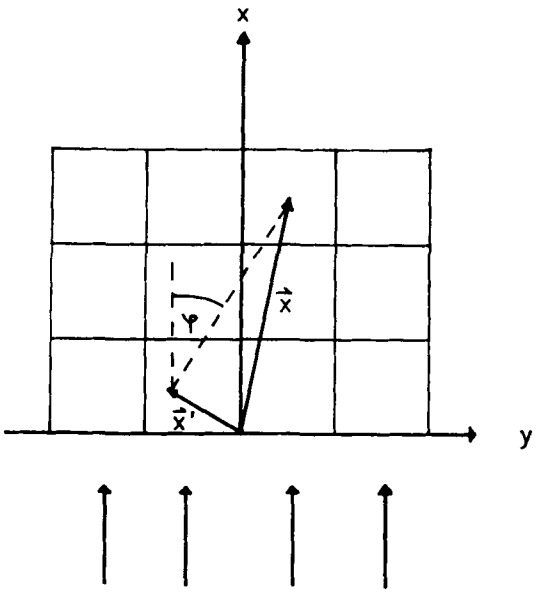

Figure 1. Plan view of the model showing the subdivision of the xy-plane into cells. The arrows indicate the direction of the incoming Rayleigh fundamental mode. Also sketched are radius vectors of a scattering point ($\mathbf{x}'$) and observation point ($\mathbf{x}$), together with the definition of the scattering angle φ.

This computational scheme may be accelerated, at some expense in terms of accuracy, by reducing the number of cells in which the wavefield is updated. For example, a factor of 2 may be gained by omitting backscattering, and a factor of 4 when scattering is limited to a ±45° cone in the forward direction, similar to the 45° approximation used in finite-difference calculations. We have not tested these alternatives on accuracy, but we guess that tapers will be necessary to avoid cut-off effects which disturb the destructive interference of the sideways-scattered waves.

5 ISOTROPIC PERTURBATIONS

In the case of isotropic heterogeneities, the perturbed elasticity tensor takes the form

$$\gamma_{ikjl} = \Delta\lambda\, \delta_{ik}\, \delta_{jl} + \Delta\mu(\delta_{ij}\, \delta_{kl} + \delta_{il}\, \delta_{kj}). \quad (19)$$

Here, $\Delta\lambda$ and $\Delta\mu$ are the perturbations of the Lamé parameters λ and μ, respectively. In the following, we consider layered media, and give expressions of the scattering kernels valid for a single layer. The scattering kernel for a whole package of layers is then simply obtained by summing over all layers.

If equation (19) is inserted into equation (14), the

single-layer scattering kernel K_P takes the form

$$K_P^{nm}(x, y \mid x', y') = -\Delta\lambda \int dz'\, \partial_i' g_i^n (\partial_3' S_3^m - ik^m S_1^m) - \Delta\mu \int dz' [\partial_3' g_j^n + \partial_j' g_3^n)\partial_3' S_j^m - ik^m(\partial_1' g_j^n + \partial_j' g_1^n) S_j^m] + \omega^2 \Delta\rho \int dz' g_i^n S_i^m. \quad (20)$$

By inserting the expressions of equation (6) for g_i and of equation (12) for S_j, explicit formulae for the scattering kernel K_P can be obtained.

Here, we focus on a special case which we consider of particular interest for practical applications: scattering of the Rayleigh fundamental mode on to itself. Then, the kernel which we denote now by K_P^{RR} may be written in the form

$$K_P^{RR}(x, y \mid x', y') = -\frac{i}{8cc_g J_1} [H_0^{(2)}(kR) \times (-\Delta\lambda R_{\lambda 0} + \Delta\rho R_{\rho 0} - \Delta\mu R_{\mu 0}) - iH_1^{(2)}(kR)\cos\varphi(\Delta\rho R_{\rho 1} - \Delta\mu R_{\mu 1}) - H_2^{(2)}(kR)\cos 2\varphi(-\Delta\mu R_{\mu 2})]. \quad (21)$$

In this equation we have introduced layer integrals by, e.g. $R_{\mu 1}$, where μ, λ and ρ indicate the elastic parameter to which the integral belongs, and the indices 0, 1 or 2 stand for the associated order of the Hankel function. R is the distance between the point (x', y') and the observation point (x, y), and φ is the scattering angle defined as the angle between the line connecting both points and the x-axis (Fig. 1). k is the wavenumber of the Rayleigh fundamental mode. The layer integrals are explicitly given by

$$R_{\lambda 0} = \int \left(\frac{dU}{dz'} + kV\right)^2 dz', \qquad R_{\rho 0} = \int \omega^2 U^2\, dz',$$

$$R_{\rho 1} = \int \omega^2 V^2\, dz', \qquad R_{\mu 0} = \int \left[2\left(\frac{dU}{dz'}\right)^2 + k^2 V^2\right] dz', \quad (22)$$

$$R_{\mu 1} = \int \left(kU - \frac{dV}{dz'}\right)^2 dz', \qquad R_{\mu 2} = \int k^2 V^2\, dz',$$

where U and V denote the eigenfunctions of the Rayleigh fundamental mode.

If we further assume the perturbations of the Lamé parameters to be constant in each cell, and define the cell integrals

$$P_\nu(p, q \mid p', q') = \frac{-i}{8cc_g J_1} \iint dx'\, dy' (-i)^\nu \times H_\nu^{(2)}(kR)\cos\nu\varphi \exp[-ik(x' - p')], \quad (23)$$

we may write the scattering kernel of a cell in the form

$$K_C^{RR}(p, q \mid p', q') = P_0[-\Delta\lambda(p', q')R_{\lambda 0} + \Delta\rho(p', q')R_{\rho 0} - \Delta\mu(p', q')R_{\mu 0}] + P_1[\Delta\rho(p', q')R_{\rho 1} - \Delta\mu(p', q')R_{\mu 1})] + P_2[-\Delta\mu(p', q')R_{\mu 2}]. \quad (24)$$

The factorization into layer and cell integrals leads to another numerical commodity. Since the cell integrals only depend on the scattering angle and the distance between scatterer and observation point, it is sufficient to compute the cell integrals on a grid large enough to encompass all possible scatterer–receiver configurations. Actually, we need to consider only one-half of the possible configurations, because of the symmetry of the cell integrals with respect to the forward direction. As well as the layer integrals, the cell integrals may be computed in advance and be used for different heterogeneous structures.

We have not yet mentioned one important detail of our numerical scheme. When evaluating the cell integrals of equation (23), we actually use the Born approximation, since neither the change of the exciting plane wave nor backscattering is taken into account. If we use a relatively coarse discretization, the Born approximation in its common linear form is not accurate enough (Snieder 1986b). We illustrate the problem with a simple example. Consider a band-like heterogeneity between $x = 0$ and $x = a$ extending to infinity in the $\pm y$-direction and being embedded in a laterally homogeneous background medium with wavenumber k. The wavenumber within the band is assumed to differ from k by a constant amount Δk. Let a plane wave $\exp(-ikx)$ be incident from $x < 0$. We show in the Appendix that, neglecting mode coupling and backscattering, the solution for $x > a$ is $\exp[-i(kx + a\Delta k)]$. It is also shown that Born single scattering yields $(1 - ia\Delta k)\exp(-ikx)$. The amplitude according to Born scattering is then $\sqrt{1 + (a\Delta k)^2}$, which is always greater than 1. We now identify the band with a row of cells and examine the amplitude as we proceed through more bands. With single scattering, the scattered waves simply add up, and the amplitude is $\sqrt{1 + N(a\Delta k)^2}$ after N bands. With multiple scattering, we use the accumulated amplitude in each step and obtain $\sqrt{[1 + (a\Delta k)^2]^N}$, an exponentially growing amplitude. The error can be reduced by choosing the cell size to be small, but this would be numerically very inefficient because the computational effort increases with the inverse fourth power of the linear cell size. We avoid this by correcting the scattered wave from each cell with the factor

$$f = \frac{1 - \exp(-ia\Delta k)}{ia\Delta k}. \quad (25)$$

This factor equals unity in the linear approximation, but converts the Born solution for the band into

$$\left[1 - ia\Delta k \frac{1 - \exp(-ia\Delta k)}{ia\Delta k}\right] \exp(-ikx) = \exp[-i(kx + a\Delta k)], \quad (26)$$

which is identical to the exact solution except for the loss of amplitude due to reflection and mode conversion at the interfaces $x = 0$ and $x = a$. This is, however, a small second-order effect that does not accumulate while the wave propagates through a homogeneous region.

6 RELATIONS TO OTHER SCATTERING APPROACHES

If we use in equation (23) the far-field approximations of the Hankel functions (Abramowitz & Stegun 1972), we obtain

from equation (24) that

$$K_C^{RR} = \frac{-i}{8cc_g J_1} \int dx'\, dy' \sqrt{\frac{2}{k\pi R}} \exp\left[-i\left(kR - \frac{\pi}{4}\right)\right] \times \exp\left[-ik(x'-p')\right]\left[-\Delta\lambda R_{\lambda 0} + \Delta\rho(R_{\rho 0} + R_{\rho 1}\cos\varphi) - \Delta\mu(R_{\mu 0} + R_{\mu 1}\cos\varphi + R_{\mu 2}\cos 2\varphi)\right]. \quad (27)$$

The expression in square brackets is identical to the Rayleigh fundamental-mode interaction term integrated over a layer given by Snieder (1986a) in his equation (29d).

If, in addition, in the square brackets of equation (27) the angular dependences are neglected, that is φ is set to zero, but the Hankel function $H_0^{(2)}$ is resubstituted for its far-field approximation, the scattering kernel takes the form

$$K_C^{RR} = \frac{-i}{8cc_g J_1} \int dx'\, dy' H_0^{(2)}(kR) \times \exp\left[-ik(x'-p')\right]\left[-\Delta\lambda R_{\lambda 0} + \Delta\rho(R_{\rho 0} + R_{\rho 1}) - \Delta\mu(R_{\mu 0} + R_{\mu 1} + R_{\mu 2})\right]. \quad (28)$$

Summing in equation (28) the expression in square brackets over all layers yields (Snieder 1986b, equation 9.4) $4cc_g J_1 k\Delta k$, where Δk is the perturbation of local wavenumber. Thus we may write the scattered potential according to equation (18) as

$$\Phi_S^{RR}(p, q) = \frac{-i}{2} \sum_{p',q'} \Phi^R(p', q') k\Delta k(p', q') \times \int dx'\, dy' H_0^{(2)}(kR) \exp\left[-ik(x'-p')\right]. \quad (29)$$

This expression is the discrete form of the equivalent integral equation to the acoustic Helmholtz equation:

$$\nabla^2\Phi^R + (k + \Delta k)^2\Phi^R = 0. \quad (30)$$

Thus several approximation methods to model surface wave propagation are covered by our formulation: (1) multiple forward scattering in an *elastic* treatment using the scattering kernel of equation (24) and the *updated* value of the wavefield to compute the scattered field; (2) multiple forward scattering in an *acoustic* treatment using the scattering kernel of equation (28) and the *updated* value of the wavefield; (3) Born single scattering in an *elastic* treatment using the scattering kernel of equation (24) and the *incoming* wavefield to compute the scattered field; (4) Born single scattering in an *acoustic* treatment, termed by Snieder (1988) the isotropic approximation, using the scattering kernel of equation (28) and the *incoming* wavefield. Furthermore, we are at liberty to use the Hankel functions or their far-field expressions, as in Snieder (1986a).

7 TEST AND COMPARISON OF THE APPROXIMATION METHODS

In this section, we shall test the following five approximation methods against an exact solution derived by Stange & Friederich (1992b) for an elastic, layered waveguide with a cylindrical inclusion:

(i) acoustic treatment with Born single scattering (isotropic approximation);
(ii) elastic treatment with Born single scattering and far-field approximation;
(iii) elastic treatment with Born single scattering;
(iv) acoustic treatment with multiple forward scattering;
(v) elastic treatment with multiple forward scattering.

In all five cases, we only consider scattering of the Rayleigh fundamental mode on to itself. Of course, we could have included coupling to higher modes in our numerical examples. But we think that the single-mode concept followed here is, in general, the only realistic way to get information about the Earth's structure from surface wave data, especially if one uses distant earthquakes for which the proposed method is tailored. Taking into account higher mode excitation for interpretational purposes would require a reliable distinction between the higher modes that are generated by the structure under investigation and those already contained in the incoming wavefield. In view of the number and density of stations currently available in Central Europe, it is doubtful whether a distinction is realistic. Since horizontal components are strongly influenced by higher modes excited by the local structure (Stange & Friederich 1992b), we only show results for the vertical component.

We have selected two different scatterers: a cylinder of radius $r = 18$ km and one of radius $r = 9.7$ km, corresponding to about two and one fundamental-mode wavelengths in diameter. The structure of the embedding waveguide is shown in Table 1. In the interior of the cylinder, the shear wave velocity is increased by 5.7 per cent in both layers. In all examples, the fundamental Rayleigh mode comes in as a plane wave of unit amplitude with the direction of propagation indicated by an arrow. In the following figures, the wavefield for the 18 km cylinder is always depicted on the left-hand side and that of the 9.7 km cylinder on the right-hand side. Moreover, the amplitude in the figures is given with respect to the incoming fundamental mode which has unit amplitude. In all examples computed by a scattering method, we sampled the diameter of the big ($r = 18$ km) cylinder by 13 cells and the diameter of the small ($r = 9.7$ km) cylinder by 7 cells. This corresponds to about 6 cells per fundamental-mode wavelength, which is a very conservative choice.

In Figure 2 we show as a reference the amplitude of vertical displacement of the *exact* wavefield at the surface of the waveguide. It was obtained by a mode-matching technique described by Stange & Friederich (1992b). The essential point of their method is that, in order to achieve a sufficiently accurate matching of the modal expansions within and outside the cylinder, it is necessary to incorporate non-propagating modes with complex wavenumbers into the modal series. For the example of Fig. 2, 20 Rayleigh modes and 14 Love modes in the 18 km case, 22 Rayleigh and 20 Love modes in the 9.7 km case, were required. Both within and outside the cylinder, the structure of the waveguide admits five propagating Rayleigh modes

Table 1. Structure of the embedding waveguide.

layer	depth [km]	v_p [m/s]	v_s [m/s]	ρ [kg/m^3]
1	0–10	5000	3000	2000
2	10–30	6000	3500	2500

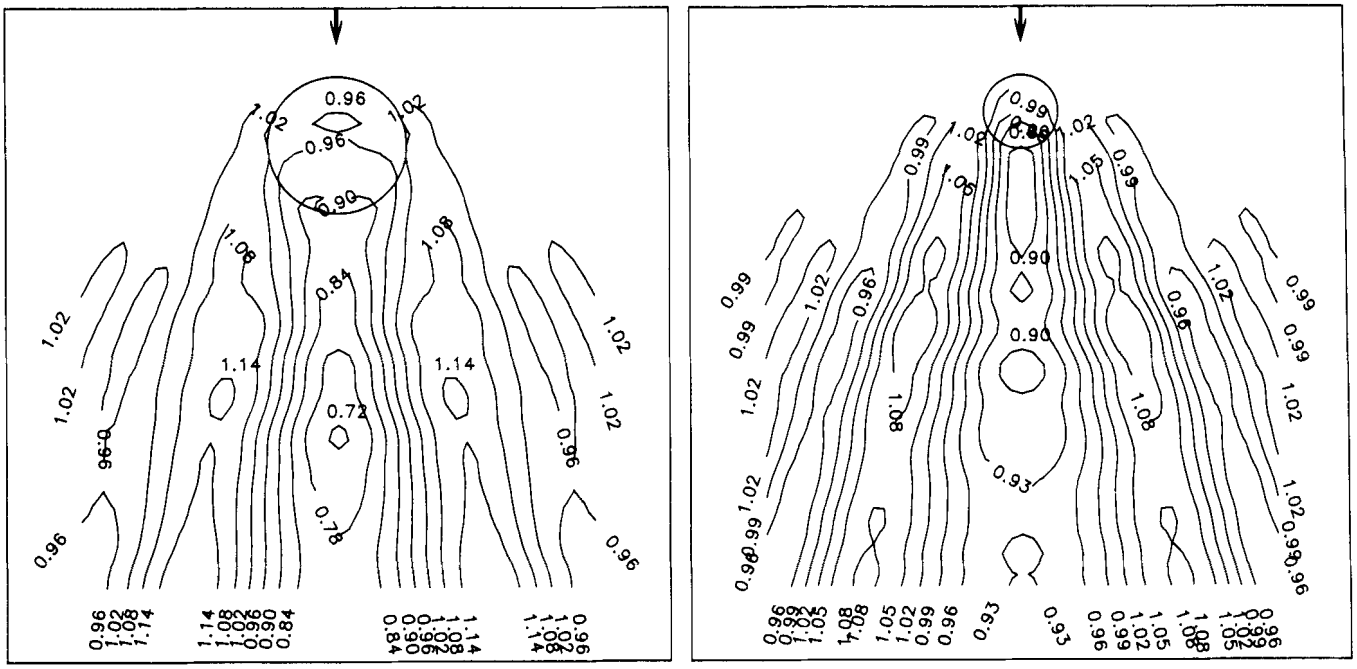

Figure 2. Amplitude of vertical displacement of the exact wavefield for a cylinder with 9.7 km radius in the right panel and for a cylinder with 18 km radius in the left panel. Involved are 20 Rayleigh and 14 Love modes in the 18 km case, and 22 Rayleigh and 20 Love modes in the 9.7 km case. The direction of the incoming fundamental Rayleigh mode which has unit amplitude is indicated by the arrow.

and three propagating Love modes. All the other modes are non-propagating modes with complex wavenumbers (for details about complex modes, see Stange & Friederich 1992a, b).

For comparison, in Fig. 3 only the contribution of the fundamental Rayleigh mode to the exact wavefield is shown. It is evident that, in spite of neglecting the contribution of the higher modes, we still obtain a very good approximation for the vertical component. The only noticeable difference is the somewhat more irregular form of the exact wavefield with its more pronounced defocusing region.

In Figs 4, 5 and 6 we show results of different approaches using Born single scattering. For the 18 km cylinder, all three single-scattering methods produce a spurious focusing zone near the end of the cylinder. It reaches its greatest

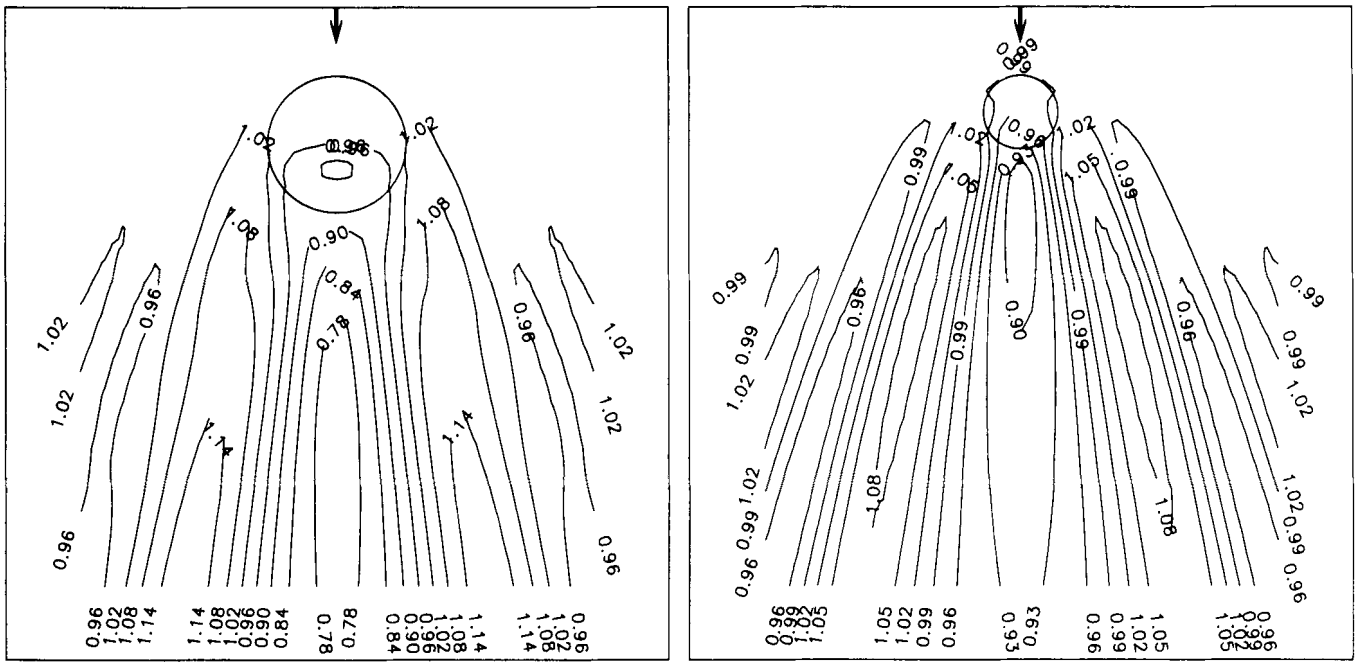

Figure 3. Amplitude of the contribution of the fundamental Rayleigh mode to the exact vertical displacement. Same arrangement as in Fig. 2.

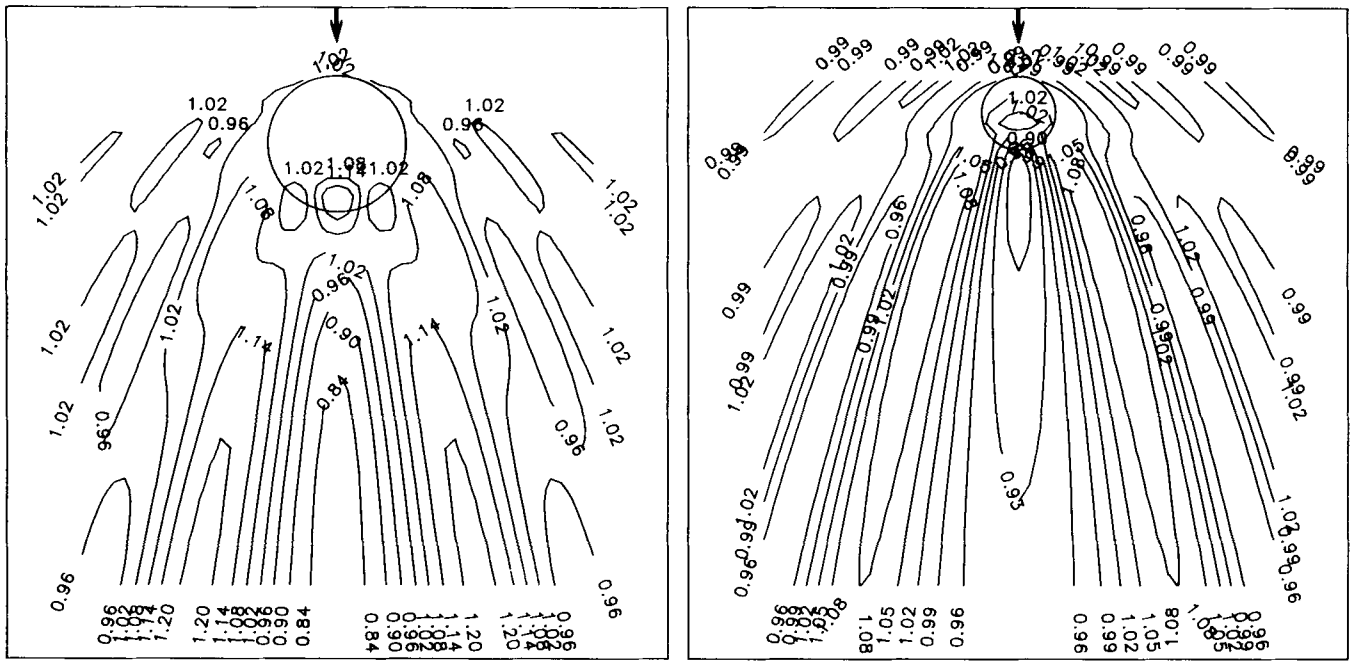

Figure 4. Amplitude of vertical displacement obtained from *single* scattering with acoustic treatment, i.e. scattering kernel evaluated according to equation (28). Same arrangement as in Fig. 2.

value for the acoustic Born method. Furthermore, the extreme values in the defocusing zone behind the cylinder and in the focusing zone at both sides are overestimated. For the 9.7 km cylinder, the agreement between elastic single scattering and the exact solution is quite good. Obviously, there is a critical scatterer size between one and two wavelengths, for which the single-scattering methods begin to yield incorrect results.

In Fig. 7, results of a computation based on an acoustic treatment including multiple forward scattering are depicted. For the big cylinder, the wavefield agrees very well with the one shown in Fig. 3, except for a small focus at the end of the cylinder. The defocusing region is slightly overestimated. On the contrary, for the small cylinder the agreement is much worse. At the far end of the cylinder, there is a steep decline of the amplitude from a nearly

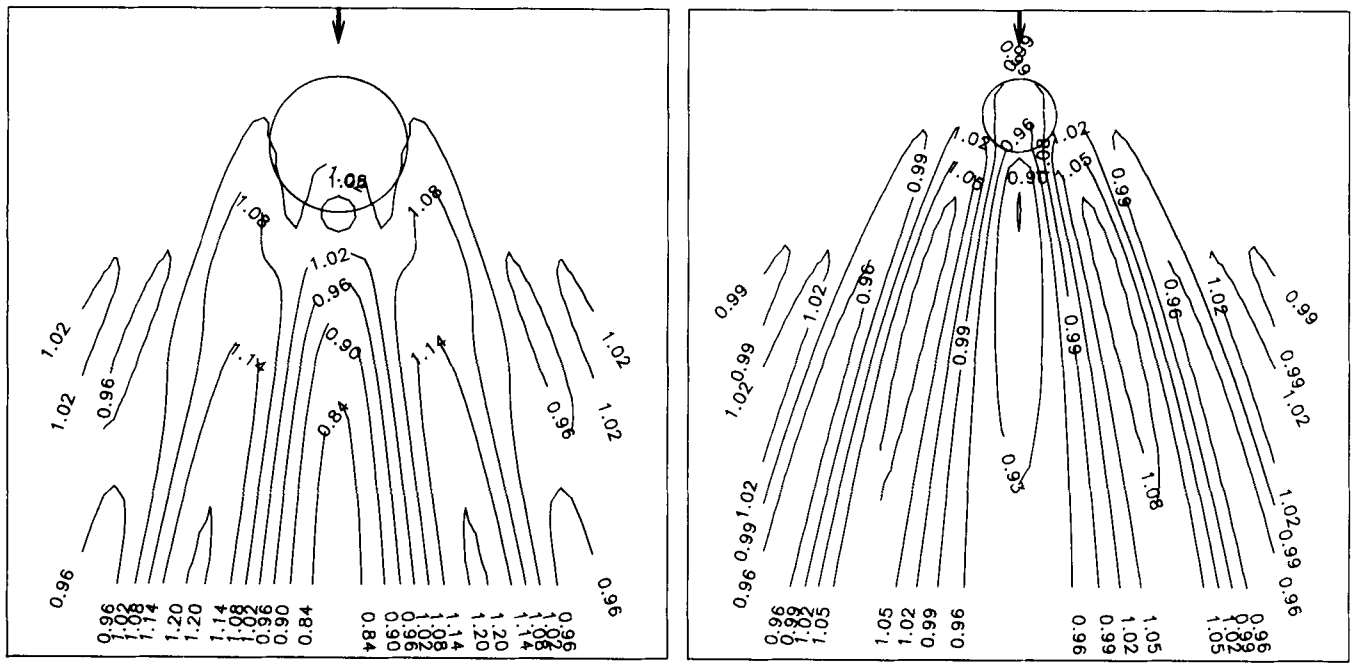

Figure 5. Amplitude of vertical displacement obtained from *single* scattering with elastic treatment but without far-field approximation, i.e. scattering kernel evaluated according to equation (24). Same arrangement as in Fig. 2.

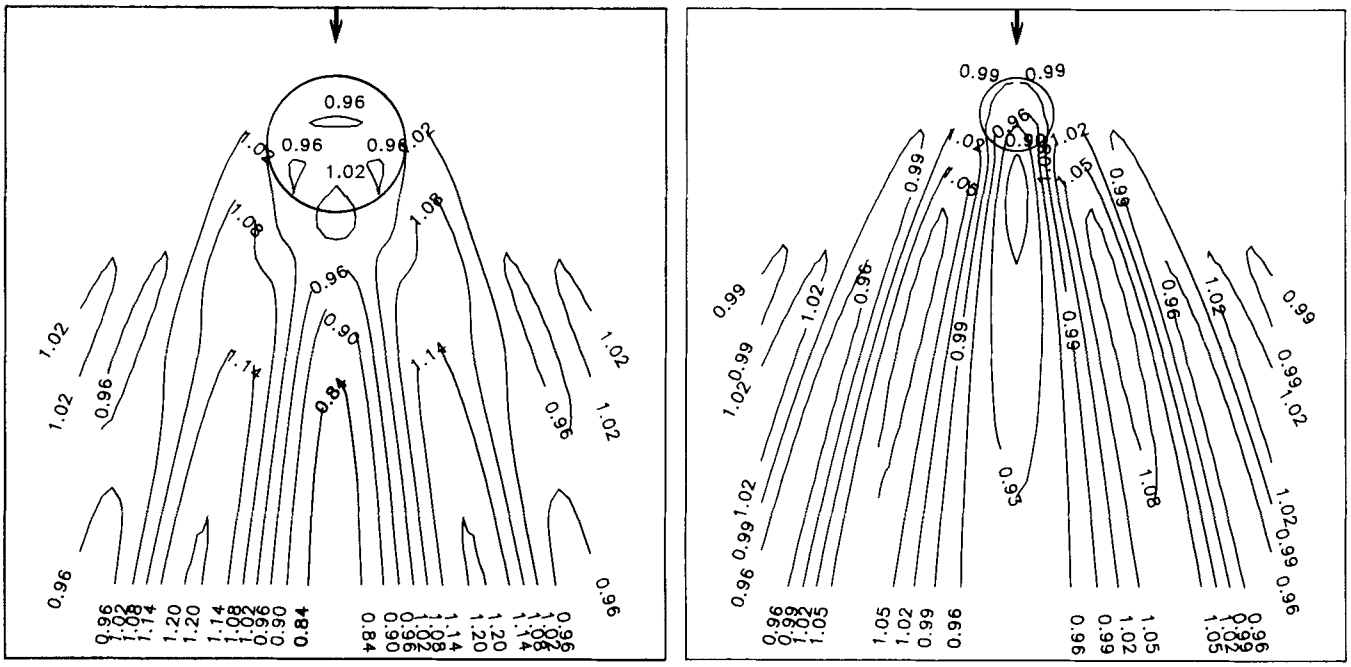

Figure 6. Amplitude of vertical displacement obtained from *single* scattering with elastic treatment and far-field approximation, i.e. scattering kernel evaluated according to equation (27). Same arrangement as in Fig. 2.

constant value within the cylinder to its lowest value in the defocusing region, while in the elastic case the transition is rather smooth. In addition, the acoustic computation yields a backscattered field which is much stronger than in the elastic case. The reason for these discrepancies is quite obvious: within an acoustic treatment the field of a point scatterer is isotropic, while in the elastic case forward scattering dominates even for a point scatterer. Thus, for small scatterers, the differences in the radiation characteristics become noticeable, while for large scatterers forward scattering is dominant in any case.

In Fig. 8 we present the results obtained with multiple elastic forward scattering as proposed in this paper. The amplitude of the potential Φ of equation (18), which is proportional to vertical displacement, is plotted. Apart from very small differences, the exact fundamental-mode

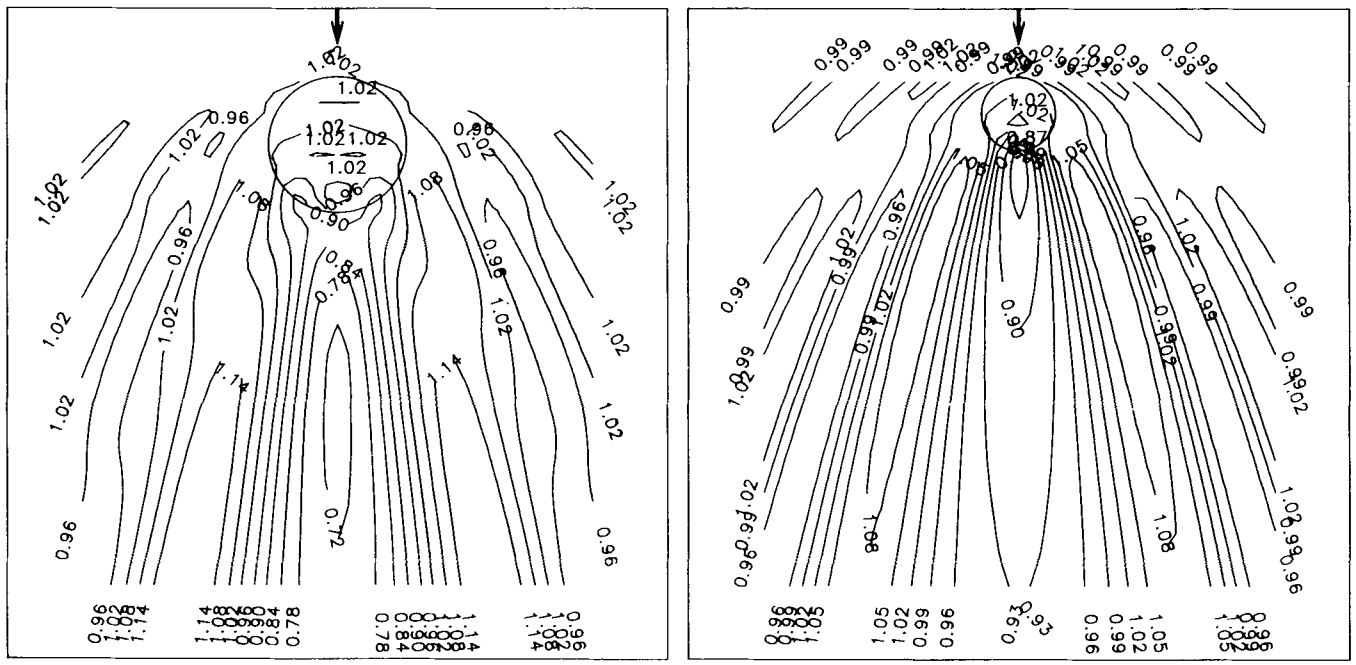

Figure 7. Amplitude of vertical displacement obtained from the *multiple* forward scattering method in the acoustic approximation. Scattering kernel evaluated according to equation (28). Same arrangement as in Fig. 2.

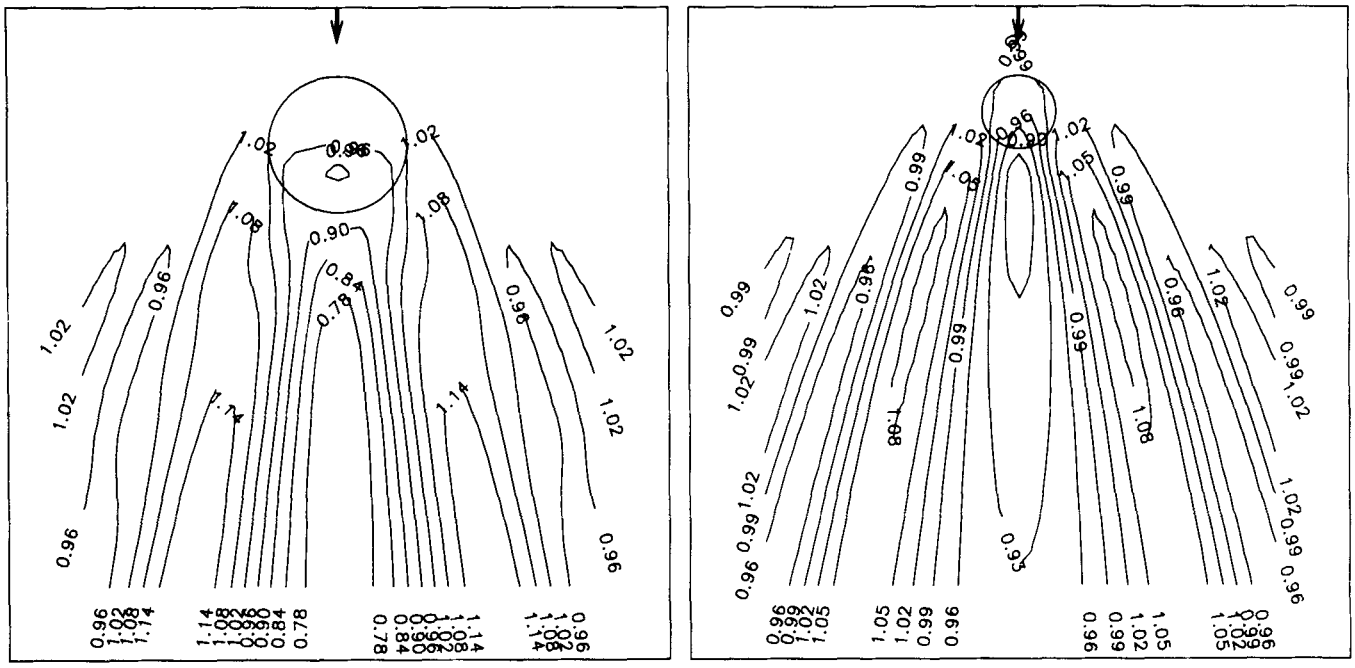

Figure 8. Amplitude of vertical displacement obtained from the proposed *multiple* forward scattering method. Elastic treatment, i.e. scattering kernel evaluated according to equation (24). Same arrangement as in Fig. 2.

displacement of Fig. 3 is reproduced by the proposed method.

To give a more precise idea of the performance of the tested methods for the big cylinder, in Figs 9 and 10 we show the amplitude of the vertical displacement for two cross-sections, one at the end of the cylinder and one far out in the far field. It is evident that the multiple forward scattering methods are much closer to the exact solution than the Born single-scattering methods.

This leads to an important conclusion. Depending on the shear wave velocity contrast, there exists a critical scatterer size above which the solutions obtained from elastic and acoustic multiple forward scattering converge to each other, while the error of the single-scattering methods increases. Below this critical scatterer size, elastic and acoustic multiple scattering diverge from each other, while the

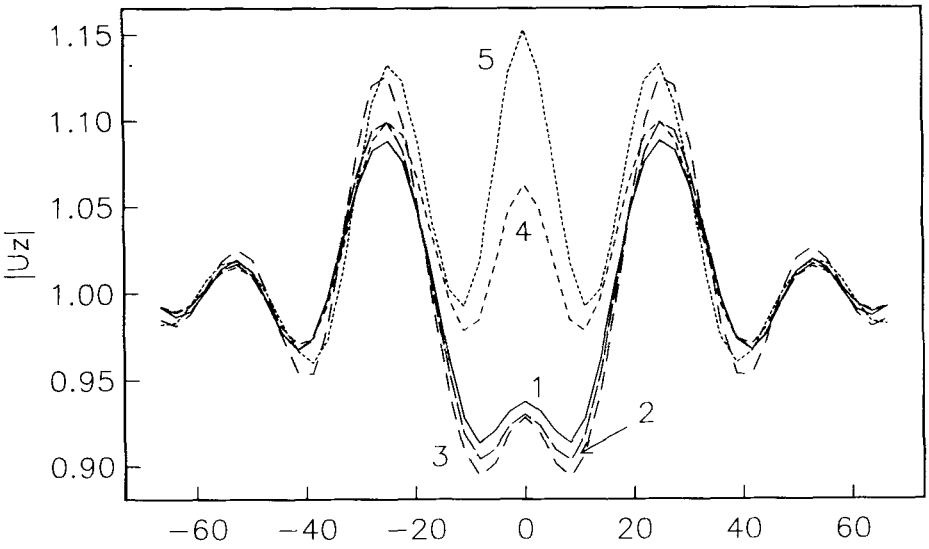

Figure 9. Cross-section of vertical displacement amplitude for the 18 km cylinder taken at a transverse profile at the end of the cylinder. The fundamental Rayleigh mode comes in with unit amplitude. The horizontal scale is in km. (1) Exact wavefield (only fundamental-mode contribution); (2) elastic treatment with multiple forward scattering; (3) acoustic treatment with multiple forward scattering; (4) elastic treatment with single scattering and far-field approximation; (5) acoustic treatment with single scattering.

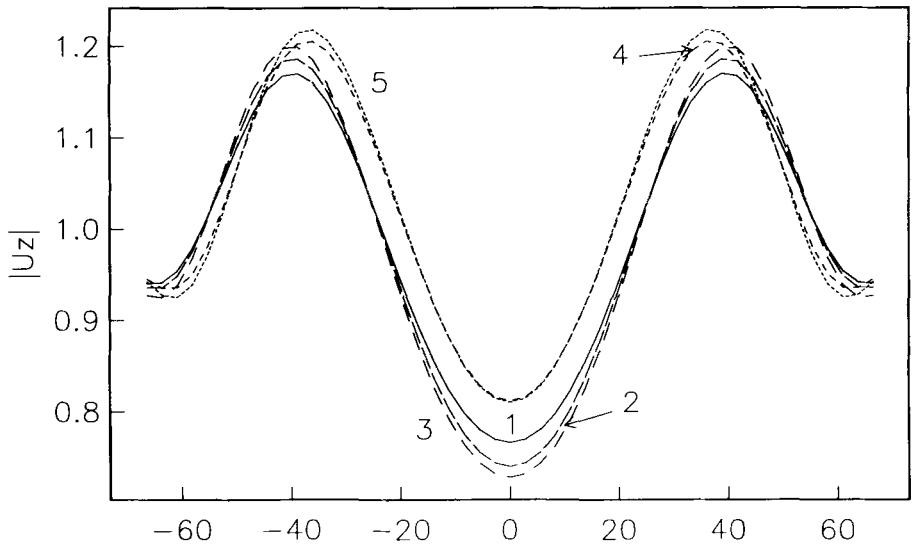

Figure 10. Cross-section of vertical displacement amplitude for the 18 km cylinder taken at a transverse profile about six wavelengths behind the centre of the cylinder. The fundamental Rayleigh mode comes in with unit amplitude. The horizontal scale is in km. (1) Exact wavefield (only fundamental-mode contribution); (2) elastic treatment with multiple forward scattering; (3) acoustic treatment with multiple forward scattering; (4) elastic treatment with single scattering and far-field approximation; (5) acoustic treatment with single scattering.

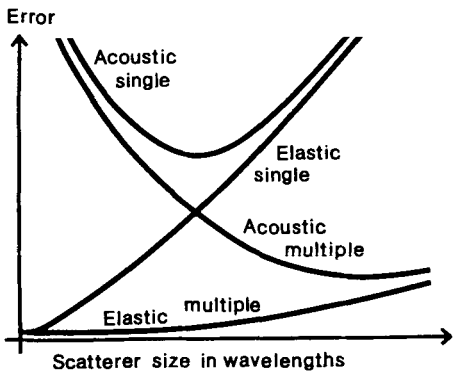

Figure 11. Qualitative behaviour of errors (therefore no scale) as a function of scatterer size for different approaches to surface wave scattering. For the velocity contrast used in the numerical examples, the horizontal axis would cover a range from zero to roughly two wavelengths.

difference between single and multiple scattering shrinks. In Fig. 11 we show a very qualitative sketch which illustrates the above discussed behaviours of the various methods.

8 CONCLUSION

There are two main results of this paper. First, by introducing potentials and assuming that the wavefield propagates roughly as a plane wave through the region of interest, which is certainly valid in teleseismic situations, we have been able to transform the elastic surface wave scattering problem of equation (11) into the form of a 2-D standard integral equation. The formulation allows an extension of the classical Born single-scattering methods to include multiple scattering in the forward direction. It is valid for fully anisotropic perturbations of the elastic parameters. Moreover, no additional numerical effort compared to single-scattering methods is required if the wavefield is to be computed over the whole anomalous region.

Subdividing the medium into cells and invoking the piecewise-plane-wave approximation, we derived a discretized form of the standard integral equation. Its kernel represents the scattered field of a cell excited by a plane wave travelling into the dominant direction of propagation. Due to the formulation in terms of a standard integral equation, the method covers several approximation schemes, depending on the kind of scattering kernel used, and on the way in which the total wavefield is approximated to compute the scattered field; for instance, multiple forward scattering with single backscattering, as well as Born single scattering of both elastic surface waves and acoustic waves. Moreover, we are at liberty to use the far-field approximations of the Hankel functions.

Secondly, the multiple-scattering methods yield nearly exact results. We have been able to test the performance of five different approximation methods against an exact solution obtained by Stange & Friederich (1992b) for a cylindrical scatterer. We found the multiple-scattering methods, in both an elastic and an acoustic treatment, superior to all Born single-scattering methods if the scatterer exceeded a critical size. Above that critical scatterer size, which in our cases lies between one and two wavelengths, the main errors are caused by the neglect of multiple scattering. Thus, depending on the kind of scatterers, even an acoustic treatment may be accurate enough to model surface wave propagation if multiple scattering is taken into account. For scatterer sizes below one wavelength, single scattering is accurate enough, but now elastic and acoustic treatments may differ considerably.

The proposed method is not only very accurate but also very efficient. For example, at a period of 50 s, if we choose the cell size to be a quarter of a wavelength, which is a very conservative choice, a grid of 20×20 cells would suffice to

cover an area of $1000 \times 1000\,\mathrm{km}^2$. Thus we also expect the multiple forward scattering method to be suited for an inversion of surface wave measurements.

ACKNOWLEDGMENTS

S. Stange was supported by the German Science Foundation (DFG, grant number Wi 1006/1-1). Computations were performed on a SUN 4/110 workstation.

REFERENCES

Abramowitz, M. & Stegun, I. A., 1972. *Handbook of Mathematical Functions*, Dover Publication Inc., New York.

Bostock, M. G., 1991. Surface wave scattering from 3-D obstacles, *Geophys. J. Int.*, **104,** 351–370.

Bostock, M. G., 1992. Reflection and transmission of surface waves in laterally varying media, *Geophys. J. Int.*, **109,** 411–436.

Gradstein, I. S. & Ryshik, I. M., 1981. *Tables of Series, Products and Integrals*, Vol. 2, Harri Deutsch, Thun.

Gregersen, S., 1978. Possible mode conversion between Love and Rayleigh waves at a continental margin, *Geophys. J. R. astr. Soc.*, **54,** 121–127.

Kennett, B. L. N., 1984. Guided wave propagation in laterally varying media—I. Theoretical development, *Geophys J. R. astr. Soc.*, **79,** 235–255.

Kennett, B. L. N. & Mykkeltveit, S., 1984. Guided wave propagation in laterally varying media—II. Lg-waves in north western Europe, *Geophys. J. R. astr. Soc.*, **79,** 257–267.

Odom, R. I., 1986. A coupled mode examination of irregular waveguides including the continuum spectrum, *Geophys. J. R. astr. Soc*, **86,** 425–453.

Snieder, R., 1986a. 3-D linearized scattering of surface waves and a formalism for surface wave holography, *Geophys. J. R. astr. Soc.*, **84,** 581–605.

Snieder, R. 1986b. The influence of topography on the propagation and scattering of surface waves, *Phys. Earth planet. Interiors*, **44,** 226–241.

Snieder, R., 1988. Large-scale waveform inversion of surface waves for lateral heterogeneity, 1. Theory and numerical examples, *J. geophys. Res.*, **93,** 12 067–12 080.

Stange, S. & Friederich, W., 1992a. Guided wave propagation across sharp lateral heterogeneities: the complete wavefield at plane vertical discontinuities, *Geophys. J. Int.*, **109,** 183–190.

Stange, S. & Friederich, W., 1992b. Guided wave propagation across sharp lateral heterogeneities: the complete wavefield at a cylindrical inclusion, *Geophys. J. Int.*, **109,** 183.

Takeuchi, H. & Saito, K., 1972. Seismic surface waves, *Methods of computational physics*, **11,** 217–295, Academic Press, New York.

APPENDIX

We derive here the surface wave field for a band-like heterogeneity between $x = 0$ and $x = a$ extending to infinity in the y-direction. The elastic parameters are assumed to vary only with respect to x. Assume an incoming plane wave propagating in the positive x-direction. Since the incoming wave and the structure depend only on x, the scattering problem is purely 1-D. The 1-D point-scattering kernel is then simply obtained by integrating K_P^{RR} of equation (21) with respect to y:

$$K_P^{1D}(x, x') = \int_{-\infty}^{\infty} dy' K_P^{RR}(x, y \mid x', y'). \tag{31}$$

After substituting $u = R^2/(x - x')^2$, the integrals over the Hankel functions can be brought into a form which may be found in Gradstein & Ryshik (1981, p. 90, 15). One obtains

$$\int_{-\infty}^{\infty} dy' H_\nu^{(2)}(kR) \cos \nu\varphi = i^\nu \frac{2}{k} \exp\left[-ik(x - x')\right]. \tag{32}$$

Together with equation (21) and the definition of Δk used in equation (29), the 1-D scattering kernel may be written in the simple form

$$K_P^{1D}(x, x') = -i\Delta k(x') \exp\left[ik(x - x')\right]. \tag{33}$$

The scattering field of the band heterogeneity is then computed from

$$\Phi_S(x) = \int_0^a dx' K_P^{1D}(x, x')\Phi(x'). \tag{34}$$

This expression is exact except for the neglect of mode coupling. If we also neglect back scattering, the contributions of the scatterers ahead of the receiver must be discarded. Thus equation (34) reduces to

$$\varphi_S(x) = \int_0^x dx' K_P^{1D}(x, x')\Phi(x'). \tag{35}$$

We follow Kennett (1984) and substitute $\Phi(x) = c(x) \exp(-ikx)$, leading to

$$c(x) - 1 = -i \int_0^x dx' \Delta k(x') c(x'), \tag{36}$$

which is equivalent to the differential equation

$$\partial_x c(x) = -i\Delta k(x) c(x), \tag{37}$$

with the initial condition $c(0) = 1$. The solution of equation (37) is

$$c(x) = \exp\left[-i \int_0^x \Delta k(x')\, dx'\right]. \tag{38}$$

Thus, if multiple forward scattering is taken into account, there is only a change in the *phase* of the wave. The amplitude remains unchanged. Assuming constant Δk, we may write, at $x > a$,

$$\Phi(x) = \exp\left[-i(kx + a\Delta k)\right]. \tag{39}$$

If we solve equation (35) with constant Δk using the Born approximation, we obtain

$$\Phi_{\mathrm{Born}}(x) = \exp(-ikx)(1 - ia\Delta k), \tag{40}$$

which is just the first-order approximation of equation (39).